Contents lists available at ScienceDirect

Transactions of Nonferrous Metals Society of China

36(2026) 956−973

www.tnmsc.cn

Mechanism of ultrasound enhanced selective oxygen pressure leaching of Ga and Ge from zinc powder replacement residue

Yuan-xin LIANG [a,b], Meng SUN [a,b], Bo-yi LUO [a,b], Biao DING [a,b,*], Zhe SHEN [a,b,**], Tian-xiang ZHENG [a,b], Qiang LI [a,b], Bang-fei ZHOU [a,b], Chun-mei LIU [a,b], Cai-gui WU [c], Wei-li REN [a,b], Yun-bo ZHONG [a,b,***]

[a] College of Materials Science and Engineering, Shanghai University, Shanghai 201900, China;
[b] State Key Laboratory of Advanced Special Steel, Shanghai University, Shanghai 201900, China;
[c] Danxia Smelter, Shenzhen Zhongjin Lingnan Nonfemet Co., Ltd., Shaoguan 512000, China

Abstract: The leaching mechanism of gallium (Ga) and germanium (Ge) from zinc powder replacement residue (ZPRR) was investigated through ultrasonic-assisted sulfuric acid leaching. Characterization via XRD, SEM, XPS, and FT-IR revealed that ultrasonic treatment promotes the dehydration of H_4SiO_4 colloids, thereby reducing their adsorption capacities for Ga and Ge complexes. Additionally, ultrasound enhances the dissolution of CaS in H_2SO_4, increasing H_2S production, which aids in the reduction of Fe^{3+} and mitigates iron precipitate formation. Process parameters including ultrasonic power (0−450 W), temperature (100−120 °C), and leaching time (30−120 min) were systematically optimized, achieving optimal leaching efficiencies of Ga and Ge at 95.7% and 94.5%, respectively.

Keywords: oxygen pressure acid leaching; ultrasound treatment; zinc powder replacement residue; gallium; germanium; leaching mechanism

1 Introduction

Gallium (Ga) and germanium (Ge) are rare metals that play a crucial role in advancing high technology due to their exceptional physical and chemical properties. They are widely used in semiconductors, optoelectronic materials, alloys, medical devices, magnetic materials, and various other industries [1−5]. Furthermore, Ga and Ge hold significant strategic and economic values as critical elements for vital sectors such as cutting-edge information technology, artificial intelligence, and robotics. It is noted that the Ge and Ga minerals are highly scarce. A substantial amount of marketable zinc was extracted from lead−zinc ore in the forms of both oxidized and sulphide ore bodies using a two-step acid leaching method. The leached residue contained a certain quantity of Ga and Ge, which could be recovered and utilized. Following the neutralization and replacement of impurity metals by adding zinc concentrates, the solid residue, referred to as zinc powder replacement residue (ZPRR), exhibited a notable increase in Ga and Ge contents [6].

Leaching Ga and Ge from ZPRR is challenging due to their tendency to exist in isomorphic forms [7,8]. The researchers proposed an atmospheric pressure acid leaching technique to study the effects of H_2SO_4 concentration, reaction time, temperature, and SO_2 pressure on the leaching efficiencies of Ga and Ge [9]. However, due to the toxicity of SO_2, the focus shifted to the use of oxygen at high pressure instead of SO_2. Consequently, the oxygen pressure

Corresponding author: *Biao DING, Tel: +86-15026981773, E-mail: dingbiao312@shu.edu.cn;
**Zhe SHEN, Tel: +86-13816906979, E-mail: xiabai@shu.edu.cn;
***Yun-bo ZHONG, Tel: +86-13636659501, E-mail: yunboz@staff.shu.edu.cn

https://doi.org/10.1016/S1003-6326(25)67009-9
Received 27 June 2024; accepted 9 May 2025

acid leaching (OPAL) method was proposed, which is not only safer, but also improves the leaching efficiencies of Ga and Ge [8,10]. As a result, the extraction efficiencies of Ga and Ge were significantly enhanced. Prior research has demonstrated that applying external factors, such as ultrasound, can effectively improve the leaching process [11,12].

Ultrasound is a high-frequency elastic mechanical vibration wave with high energy density. In recent decades, ultrasound has been used to improve the extraction of valuable metals from rare-earth ores, industrial wastes, and end-of-life lithium-ion battery waste [13−15]. The cavitation, mechanical, and thermal impacts of ultrasound can enhance leaching recovery, reduce leaching time, and minimize waste. Ultrasound-assisted leaching techniques can significantly decrease leaching time when compared to traditional leaching methods [16]. Ultrasonic waves in a liquid medium generate cavitation bubbles through alternating positive and negative pressures. When these bubbles collapse, they produce high temperatures, high pressures, and micro-jets in the liquid, enhancing mass transfer by promoting phase interface renewal and interfacial perturbation [17]. Furthermore, ultrasound can significantly enhance the leaching efficiency and reaction rate of impurities in aphanitic graphite by reducing particle size, removing the passivation layer, and increasing mass transfer rate through cavitation-induced mechanical, chemical, and thermal effects [18]. It is important to note that advancements have been made in utilizing ultrasound in reaction processes. Researchers have extensively studied the use of ultrasound to assist in synthesis, stripping, and product functionalization [19−22]. A cost-effective and simple technique was proposed to synthesize graphene from graphite in ethanol using ultrasound-assisted curcumin. This method not only enables the exfoliation of graphite into graphene but also produces graphene−curcumin blends, which have potential applications in the pharmaceutical industry. However, there has been limited research on the use of ultrasound to improve the leaching process of ZPRR. Therefore, further exploration is required to determine optimal conditions for leaching, such as temperature and ultrasonic power.

This study thoroughly investigated the mechanism of Ga and Ge leaching from ZPRR using an ultrasonic field-enhanced selective OPAL process. The following aspects were examined in this study: (1) Selective leaching of Ga and Ge, including the influence of temperature and ultrasonic power; (2) Optimization of leaching conditions for Ga and Ge recovery and elucidation of the underlying leaching mechanisms; (3) The role of the ultrasonic field in the intrinsic mechanism of the leaching process. The findings of this study offer a sustainable and effective approach to enhance the leaching efficiencies of Ga and Ge in the industrial sector.

2 Experimental

2.1 Material preparation and leaching experiment procedure

The leaching experiments were conducted in a 400 mL sealed, high-pressure reactor, internally coated with polytetrafluoroethylene to protect the reactor wall from acid corrosion. The temperature was elevated to a pre-established range (100−150 °C) using a numerical control power supply, and the reactor was heated using a furnace tube equipped with a resistance wire. External circulation of high-purity oxygen (Stable at 0.5 MPa after heating to a specified temperature) was employed to enhance the effectiveness of the leaching process. Before heating, ZPRR and a certain concentration of sulfuric acid (15 and 150 g/L H_2SO_4 for targeted extraction of Ge and Ga, respectively) were poured into the reactor. The reactor was then tightly sealed, and the stirrer was activated at a speed of 400 r/min. The leaching experiment was enhanced by employing the FS−450N ultrasonic treatment device (Shanghai Yanzheng Experimental Instrument Co., Ltd.). A port at the bottom of the reactor corresponds to the size of the ultrasound probe and a sealing ring to prevent liquid leakage. The ultrasonic frequency remained consistent at 20 kHz, while the ultrasonic power could be varied between 0 and 450 W. The ultrasonic device was activated to initiate the leaching experiments.

At the end of the experiment, the leach residue was filtered by the SHZ-D circulating water vacuum pump (Shanghai Huichuang Chemical Instrument Co., Ltd.), and the separated solid residue was dried in an 101-0B oven (Dongguan Huatong Instrument Equipment Co., Ltd.) and weighed for subsequent characterization.

The chosen original material for this research

was ZPRR, which underwent treatment by a corporation. Subsequently, it was dried and ground to a particle size of larger than 48 μm for experiment purposes. The experiment involved diluting sulfuric acid (H_2SO_4, 98%, China National Pharmaceutical Group) with deionized water to concentrations of 15 and 150 g/L, respectively. The specific experimental procedure was as follows: The ZPRR was dried, and a portion was leached with 15 g/L H_2SO_4 using the OPAL method. After the leaching reaction, the solution was filtered, the solid was removed and dried, and Ge content remaining after the reaction was determined by ICP. Another portion was leached with 150 g/L H_2SO_4, and the procedure mentioned above was repeated using the OPAL method.

Smaller residue particles enhance the surface area available for reaction in the acid solution, leading to improved reaction efficiencies of Ga and Ge. The effect of different particle sizes on leaching efficiency was explored. We sieved ZPRR with different meshes and found that the leaching efficiencies of Ga and Ge increased with the increase in the ZPRR size. However, when the ZPRR size was greater than 74 μm, the increase in the leaching efficiencies of Ga and Ge was not obvious (Fig. S1 in Supplementary Materials (SM)). So, it was determined that the ZPRR should be sieved with a mesh screen of pore size being 74 μm.

Therefore, the ZPRRs used in the subsequent experiments were sieved with a pore size of 74 μm.

2.2 Calculation of leaching efficiency

The leaching efficiency was calculated from the difference in elemental contents of Ga and Ge in ZPRR before and after the reaction. The formula is shown in Eq. (1) [13]:

$$x = \frac{\alpha \cdot N - \beta \cdot n}{\alpha \cdot N} \times 100\% \quad (1)$$

where the x represents the leaching efficiency of Ga or Ge; α represents the mass fraction of Ga or Ge in the original ZPRR; N represents the total mass of the original ZPRP; β represents the mass fraction of Ga or Ge in the leaching residue after the reaction; n represents the total mass of the leach residue. Each set of experimental condition parameters was replicated three times to ensure the reproducibility of the experimental data.

2.3 Characterization methods

The laser particle size analyzer (Mastersizer 2000, Malvern Instruments Ltd., UK) was used to measure the particle size of diverse samples. The inductively coupled plasma spectroscopy (ICP-OES, AGILENT ICP-OES 730) was employed to analyze the chemical composition of elements in ZPRR. The micro-zone composition of the surface of solids (feed material and leach residue) was analysed using electron probe microanalysis (EPMA, Shimadzu−1720). The morphology of leach residue was examined using scanning electron microscopy (SEM, VEGA 3 Easy Probe) under various conditions. At the same time, the elemental distribution on the surface of ZPRR was observed using energy-dispersive X-ray spectroscopy (EDS, VEGA 3 Easy Probe). The mineralogical composition of the leaching residue was investigated through the utilization of X-ray diffraction (XRD, EMPYREAN). Furthermore, the raw material and leached residue was subjected to Fourier transform infrared spectroscopy (FT-IR, NICOLET) analysis to identify the specific functional groups present in the samples before and after the reaction. The changes in elemental valence states in the residue were determined by X-ray photoelectron spectroscopy (XPS, DIONEX AQUION) before and after the leaching reaction.

The alterations in the valence states of the elements in the residue were ascertained through the utilization of XPS of the solid samples before and after the leaching reaction.

3 Results and discussion

3.1 Phase analysis results of original residue

The original ZPRR phase was analyzed using XRD, as shown in Fig. 1. The ZPRR primarily consists of $CaSO_4$, $PbSO_4$, SiO_2, and a small amount of CaS. The leaching behavior of ZPRR at various locations is greatly influenced by the nature and composition of the mineral phases [23−25].

SEM analysis, equipped with EDS, was used to examine the enrichment of the original ZPRR phase, as depicted in Fig. S2 in SM. The primary components of the original ZPRR surface are $CaSO_4$ and $PbSO_4$. Additionally, there are areas with high contents of iron-based compounds and specific Cu and Al compounds.

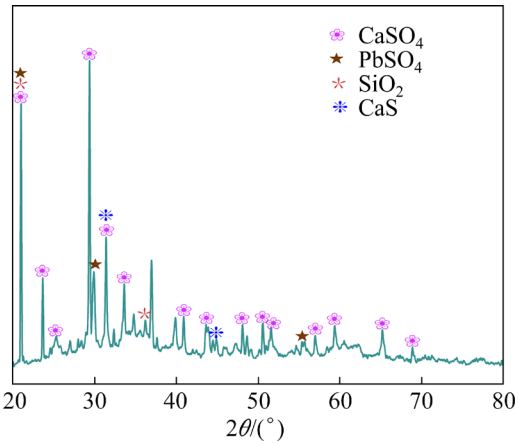

Fig. 1 XRD pattern of original ZPRR

The chemical composition of the original ZPRR was determined using different methods, in which the Ga and Ge contents were measured by ICP-OES, and the major elements were determined by EDS. Table 1 [26] presents the elemental composition of ZPRR, revealing that the original ZPRR contains a significant amount of sulfides and oxides.

Table 1 Chemical composition of ZPRR (wt.%) [26]

O	Ca	S	Cu	Zn	Pb	Si	Fe	Al	Ga	Ge
44.6	14.5	13.9	12.1	5.9	3.5	2.5	1.2	1.1	0.5	0.2

The micro-regions within the residue were analyzed using EPMA. Eight spots were randomly selected, as shown in Fig. 2. The corresponding EPMA results are presented in Table S1 in SM. Based on the data in Fig. 3, the linear regression results demonstrate a strong correlation between contents of Ga and Ge with contents of Si and Fe. This indicates that Ga and Ge are not uniformly distributed in the ZPRR, but concentrated in the Fe-rich and Si-rich phases, making them resistant to leaching.

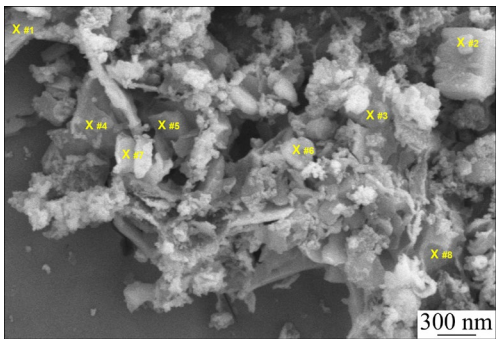

Fig. 2 EPMA image of ZPRR

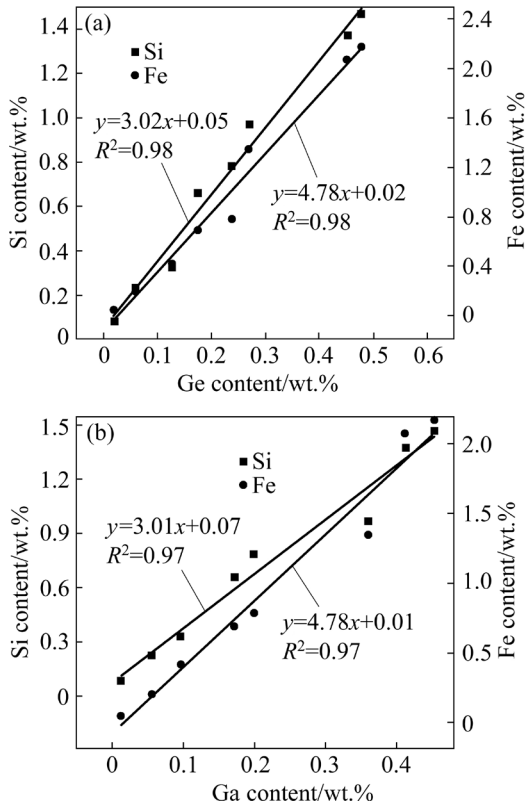

Fig. 3 Correlation curves of Si and Fe contents with Ge (a) and Ga (b) contents

The Ga and Ge occurrence states, as indicated in Table 2, were determined through selective dissolution. It is worth noting that the valence states of Ge are Ge(IV) and Ge(II), where Ge(IV) primarily consists of GeO_2, Ge_2O_3, and Ge(II) primarily consists of GeO. The valence state of Ga is Ga(III), which mainly consists of Ga_2O_3. Ga and Ge were predominantly in the oxidation state (Ga ~ 65.8%; Ge ~ 53.3%) but also in the vulcanized, mixed and elemental states. To represent the leaching process of Ga and Ge in H_2SO_4 more clearly, Tables S2 and S3 in SM were obtained.

Combining the elemental characteristics of Ga and Ge reveals that Ga and Ge can replace Fe^{3+} in minerals and exhibit an affinity for iron during the original ZPRR mineralization phase due to the similar ionic radius of Ge^{4+} and Fe^{3+}. However, Ga and Ge typically coexist harmoniously as isomorphous, resulting in challenges during leaching [27].

3.2 Solvent selection principles

Figure 4 displays the solubility and reaction extent comparison of various Ga and Ge phases

Table 2 Ga and Ge occurrence states

Ga occurrence state	Content/wt.%	Proportion/%	Ge occurrence state	Content/wt.%	Proportion/%
Oxidation state*	0.23	65.8	Oxidation state**	0.11	53.3
Vulcanized state	0.06	12.2	Vulcanized state	0.02	8.6
Mixed state	0.08	17.3	Mixed state	0.07	31.9
Elemental state	0.02	4.7	Elemental state	0.01	6.2

*: Ga_2O_3; **: GeO_2, Ge_2O_3, and GeO

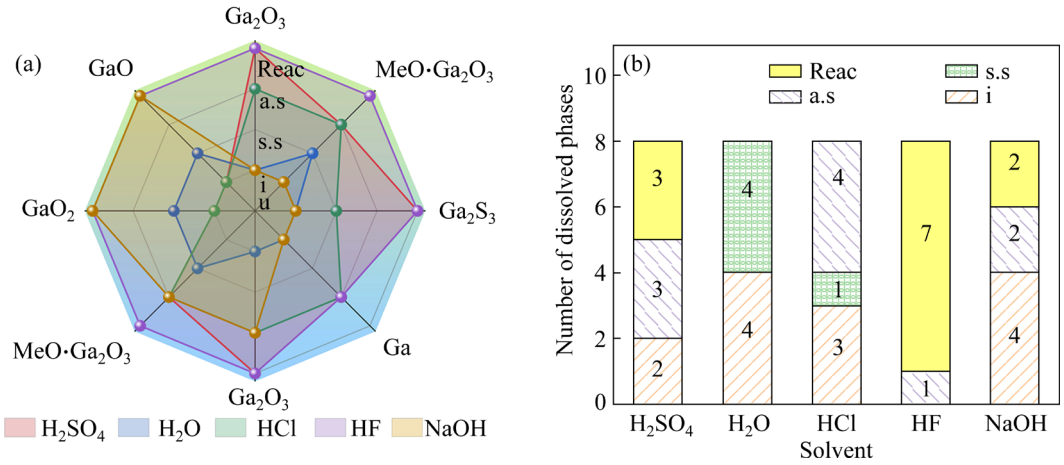

Fig. 4 (a) Solubility and degree of reaction for physical phases of Ga and Ge in different solutions; (b) Number of soluble phases in different solutions at 25 °C [28−31] ("u" represents "uncertainty"; "i" represents the term "insoluble"; "s.s." is an abbreviation for slightly soluble; "a.s" stands for "almost soluble"; "reac" stands for the process of "reacting with the solvent")

under different conditions [28−31]. H_2SO_4 is a more effective solvent for leaching Ga and Ge. Therefore, the sulfuric acid method was employed to leach Ga and Ge in all subsequent studies.

LIANG et al [26] demonstrated that leaching Ga and Ge using a two-stage OPAL method yielded more favorable results. However, determining the apparent activation energies of Ga and Ge leaching proved challenging. Consequently, we opted to separately leach Ga and Ge at different acid concentrations and calculate their respective apparent activation energies using a one-stage acid leaching method.

To examine the sequence and viability of Ga and Ge leaching in the OPAL, Figs. 5(a, b) illustrate φ−pH (φ is the potential) diagrams for the Ga−H_2O and Ge−H_2O aqueous systems using data from thermodynamic manuals, respectively [32]. In the ZPRR, the predominant forms of Ga and Ge are GeO_2, Ga_2O_3, and their corresponding minerals. In acidic conditions, Ga mostly exists as Ga^{3+}, whereas Ge is largely present as Ge(IV) cations, including Ge^{4+}, $Ge(OH)^{3+}$, $Ge(OH)_2^{2+}$, and $Ge(OH)_3^{+}$.

From a thermodynamic perspective, the order of metal oxide acid leaching, ranked from the easiest to the most difficult, is as follows: ZnO > FeO > CuO > Ga_2O_3 > Fe_2O_3 > GeO_2. As shown in Fig. 5(c), GeO_2 exhibits a larger stable phase region compared to GeO. The solubility of both GeO and GeO_2 can be enhanced with appropriate acid concentrations. However, if the H_2SO_4 concentration continues to increase, Ge^{4+} will precipitate again as H_2GeO_3 [33]. Consequently, the solubility of GeO_2 initially increases and then decreases in an acidic environment [34−36]. Considering Figs. 5(c, d) and previous research [26], we conclude that Ge can be leached separately from ZPRR in a solution of 15 g/L H_2SO_4. The declining trend of Ge solubility in a 150 g/L H_2SO_4 solution is already evident, enabling the determination of more precise activation energy values through leaching Ga in this particular environment.

3.3 Selection of leaching temperature

The temperature of a chemical reaction plays a crucial role in affecting the efficiency and extent of

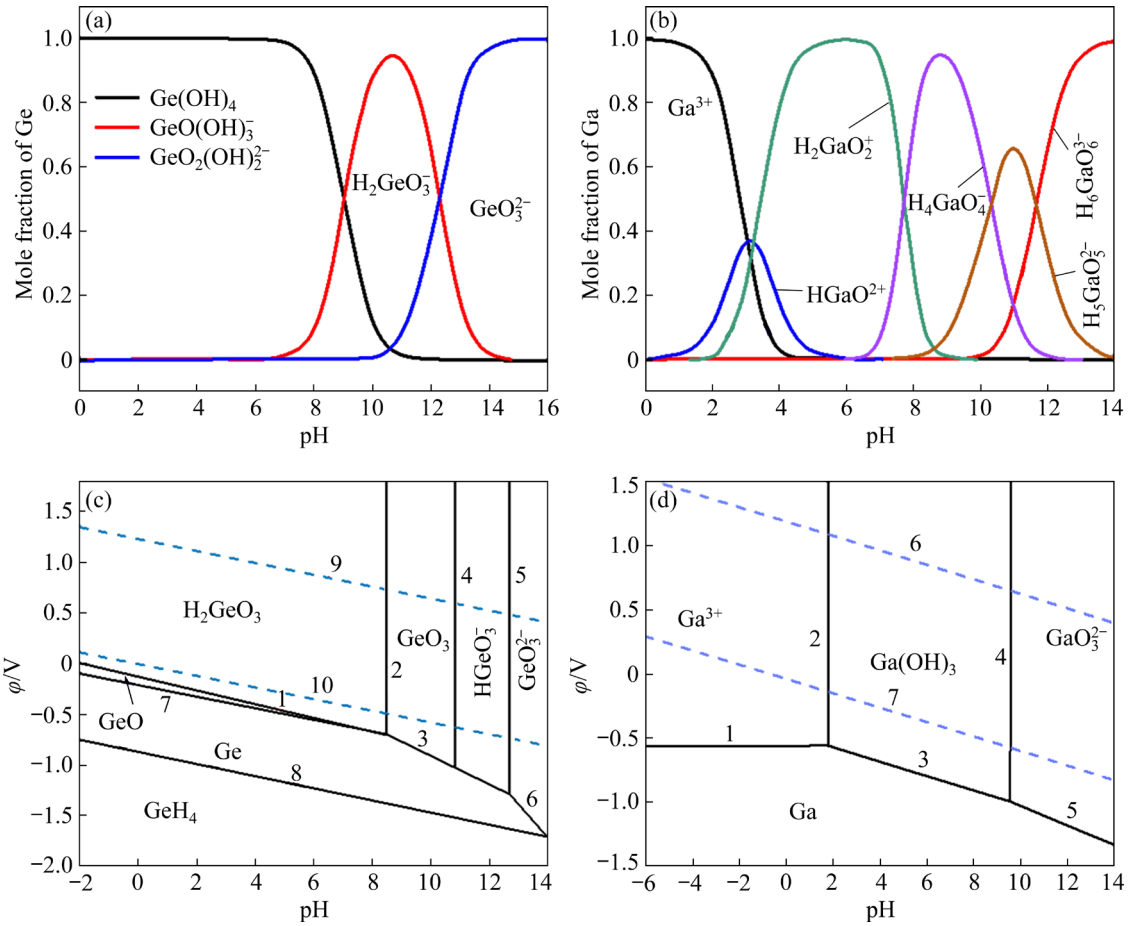

Fig. 5 Stabilized phases of Ge (a) and Ga (b) at different pH; φ−pH diagrams of Ge−H_2O (activity α=1, 0.6 MPa, 25 °C) (c) and Ga−H_2O (α=1, 0.6 MPa, 25 °C) (d) (Numbers 1−10 in (c) and 1−7 in (d) correspond to the reaction numbers in Tables S2 and S3 in SM, respectively) [1,32]

the reaction. The decrease in temperature is expected to result in a reduction in the leaching efficiencies of Ga and Ge. In the study conducted by XIN et al [37], the leaching efficiencies of Zn and Ge was investigated by the OPAL method combined with an ultrasonic field, using water-bath heating. The leaching temperature ranged from 50 to 90 °C, and the leaching efficiency of Ge increased with the increase of temperature. Even at 90 °C, the leaching efficiency of Ge was only 90%, indicating room for further improvement. HE et al [38] studied the effect of high-pressure acid leaching on the leaching efficiencies of Ga and Ge. Leaching temperatures between 100 and 150 °C were more suitable for industrial production, and the leaching efficiencies of Ga and Ge were significantly improved compared to water bath heating. However, as the temperature exceeded 150 °C, the increase in the leaching efficiencies of Ga and Ge decreased notably. Additionally, extremely high temperatures could reduce the effectiveness of the filtrate as it passes through the filter membrane [39]. This can significantly reduce the economic benefits resulting from industrial manufacturing.

Higher temperatures reduce the effectiveness of ultrasound-induced leaching enhancement on ZPRR. This phenomenon occurs because elevated temperatures influence cavitation effects, leading to the incomplete collapse of cavitation bubbles. Additionally, when the temperature is above a specific limit, the ultrasonic intensity decreases. As a result, the refraction angle of the ultrasonic probe increases, causing greater attenuation of ultrasound propagation in the liquid [40]. Consequently, the experimental parameters were designed to cover a temperature range of 100−150 °C.

Figure 6 demonstrates that temperature, leaching time, and ultrasound influence the leaching efficiencies of Ga and Ge. The sulfuric acid concentrations for selective leaching of Ge and Ga

were 15 and 150 g/L, respectively. The process was conducted under an oxygen pressure of 0.5 MPa, a stirring speed of 400 r/min, a L/S ratio of 10 mL/g, and a leaching time of 0−300 min. The leaching efficiencies of Ga and Ge were significantly increased with the application of 360 W in the ultrasonic field. At 150 °C, the leaching efficiencies of Ga and Ge reached 95.1% and 94.5%, respectively. This is because ultrasound propagates through an elastic cavitation medium and generates a cavitation process through shock waves and micro-jets, which enhances the rate of chemical reactions and improves overall reaction efficiency.

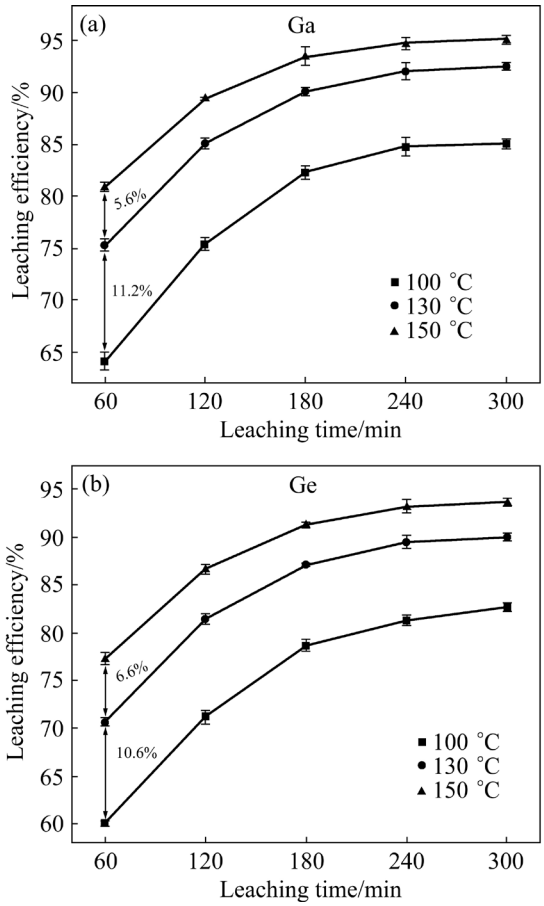

Fig. 6 Influence of leaching temperature on leaching efficiencies of Ga (a) and Ge (b) under 360 W ultrasonic field (The sulfuric acid concentration was 150 and 15 g/L, respectively, the oxygen pressure was 0.5 MPa, the stirring speed was 400 r/min, and the L/S ratio was 10 mL/g)

Cavitation bubbles can generate rapid intra-particle collisions in liquid−solid slurries, creating numerous micropores on the solid surface and facilitating the penetration of the solution into the solid interior [41]. Ultrasound treatment is a sonic process that does not introduce new impurity ions into the solution, simplifying subsequent recovery and extraction. The leaching efficiencies of Ga and Ge without ultrasound treatment are shown in Fig. S3 in SM. It is evident that the enhancement of Ga and Ge leaching gradually decreases with the increase of temperature under a 360 W ultrasonic field at the leaching time of 60 min. The leaching efficiencies of Ga and Ge are enhanced by 11.2% and 10.6%, respectively when the leaching temperature is raised from 100 to 130 °C. However, when the temperature is increased from 130 to 150 °C, the leaching efficiencies of Ga and Ge are only enhanced by 5.6% and 6.6%, respectively. On the other hand, when the leaching temperature is increased from 100 to 130 °C without applying the ultrasonic field, the leaching efficiencies of Ga and Ge are increased by 8.8% and 11.3%, respectively. From 130 to 150 °C, the leaching efficiencies of Ga and Ge are increased by 12.1% and 11.0%, respectively (see Fig. S3 in SM). These results demonstrate that ultrasound can enhance the leaching degree within a shorter leaching time and improve the leaching efficiencies of Ga and Ge more rapidly.

On the other hand, it demonstrates a constraint effect between the temperature and the impact of ultrasound, and the enhanced effect of ultrasound weakens when the leaching temperature is too high. This may be because lower temperatures promote the formation of cavitation bubbles. An increase in the specific heat ratio of the gas reduces the maximum pressure during bubble collapse [42,43]. Ultrasound primarily facilitates the leaching process by generating cavitation bubbles that expand and collapse, generating pressure to break down the residue and agitate the solution to disperse the particles. Excessive temperatures hinder the formation of cavitation bubbles. At the same time, as ultrasonic power increases, the ultrasonic density also rises, which enhances the thermal effect in the solution, leading to the loss of part of the acoustic field energy as thermal energy, reducing the acoustic energy of the oxidation reaction, which is detrimental to the process [44]. After 240 min of leaching, the leaching efficiency nearly ceases to increase.

3.4 Determination of ultrasound parameters

We investigated the impact of varying ultrasound powers (maintaining a constant ultrasound frequency

of 20 kHz) on the leaching efficiencies of Ga and Ge at 100 °C (Fig. S4 is SM).

The liquid−solid ratio was 10 mL/g, the oxygen pressure was 0.5 MPa, the stirring speed was 400 r/min, and leaching time was 240 min. Increasing the ultrasonic power significantly enhanced in the leaching efficiencies of Ga and Ge. Higher ultrasonic power reduces resistance to mass transfer through the product layer, improving reaction efficiency. The diffusion process between the solid and liquid phases is hindered by the migration of ions from the ZPRR surface into the liquid, primarily due to resistance caused by the product layer and insoluble substances. Ultrasonic power is well known for its ability to generate cavitation. This removes material from a solid surface and induces turbulence, creating highly reactive surfaces [45]. Additionally, the mechanical impact of ultrasound promotes the continuous formation of cracks and new reactive interfaces on the surface of slag, thereby enhancing the leaching reaction [44].

However, when the ultrasonic power exceeded 360 W, the leaching efficiencies of Ga and Ge showed a declining trend. Excessive power hindered the removal of impurities from the residue. This occurred because cavitation in the solution reached its limit, resulting in the accumulation of numerous small cavitation bubbles on the solid surface, which impaired the reaction efficiency at higher ultrasonic powers. Consequently, the transmission of ultrasound into the liquid was disrupted [46]. Furthermore, a continuous increase in ultrasonic power may lead to the dissolution of soluble substances in the ZPRR, forming a significant amount of fine residue that covers the surfaces of Ga and Ge. This impedes the dissolution reactions of Ga and Ge, potentially explaining the aforementioned phenomenon.

Thus, the optimal ultrasonic power was identified as 360 W, and all subsequent studies were conducted using this power level to investigate other variables. XU et al [32] explored the use of ultrasonic technology to improve the efficiency of low-grade hydrazine sulfate acid leaching of Ge. The study showed that the ideal ultrasonic power for this process was 300 W, which is consistent with our finding of optimal ultrasonic power. Ultrasound is an acoustic wave that does not introduce impurity ions into the solution, making it a convenient method for future recovery and extraction processes.

In ultrasonic-enhanced selective leaching of ZPRR, there is a governing relationship between ultrasonic power and leaching temperature. If the leaching temperature is too high, the cavitation effect of ultrasound is weakened. The optimal leaching enhancement effect is achieved at a reaction temperature of 150 °C and an ultrasonic power of 360 W. Under the optimal leaching conditions, the leaching efficiencies of Ga and Ge are 95.7% and 94.5%, respectively. Table S4 in SM further details the relevant equilibrium states of Ga and Ge in the optimal environment along with specific leaching information.

3.5 Characteristics of ZPRR after leaching

3.5.1 XRD patterns

Figure 7 displays the XRD patterns of ZPRR after common leaching at different temperatures. Figure 7(a) is obtained using a concentration of 15 g/L H_2SO_4 and a leaching time of 240 min. It is evident that at 100 °C, CaS and ZnS still exhibit prominent peaks, while the peaks of $CaSO_4$ are less pronounced. However, when the leaching temperature exceeds 130 °C, the intensity of the peaks for CaS and ZnS decreases. In contrast, the intensity of the peaks for $CaSO_4$ noticeably increases, which is because CaS in the 15 g/L of sulfuric acid occurred as follows [47]:

$$CaS+H_2SO_4=CaSO_4+H_2S,\ \Delta G=-136.0\ \text{kJ/mol} \quad (2)$$

The absence of CaS and ZnS peaks in Fig. 7(b) suggests that the 150 g/L H_2SO_4 may completely dissolve CaS and ZnS. Furthermore, the increased intensity of the $CaSO_4$ peaks indicates the occurrence of sulfide conversion reactions.

Figures 7(c, d) display the XRD patterns of ZPRR after leaching without or with the application of 360 W enhanced OPAL at 150 °C. The intensity of the $CaSO_4$ peaks increased, indicating that ultrasound promoted Reaction (2).

3.5.2 SEM images

Figure 8 compares the effect of applying an ultrasonic field on the morphology of ZPRR at a temperature of 100 °C, a sulfuric acid concentration of 15 g/L, and a reaction time of 240 min. Figure 8(a) reveals a distinct corrosion layer on the surface of the ZPRR. Despite the reaction, the surface remains relatively dense, with a thick product layer attached. This layer acts as a barrier, preventing further acid

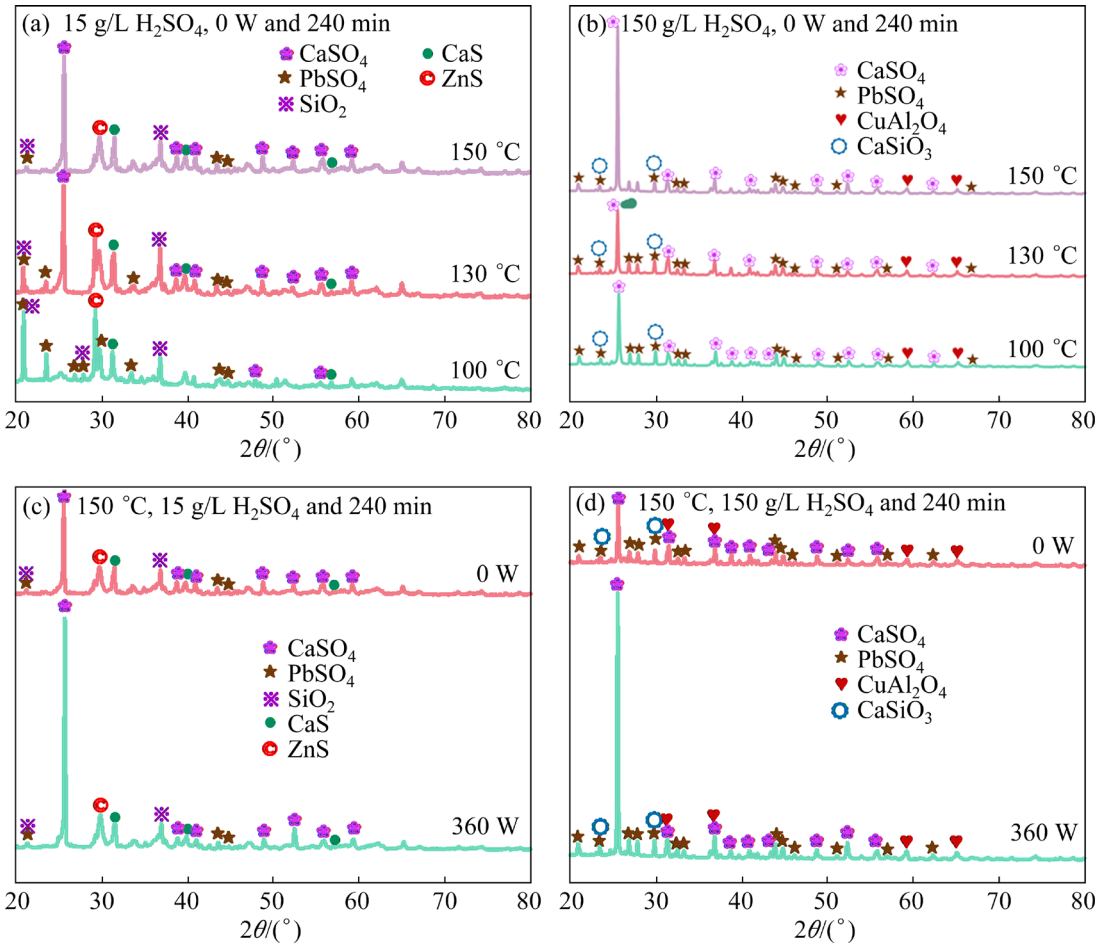

Fig. 7 XRD patterns of ZPRR after leaching under different conditions

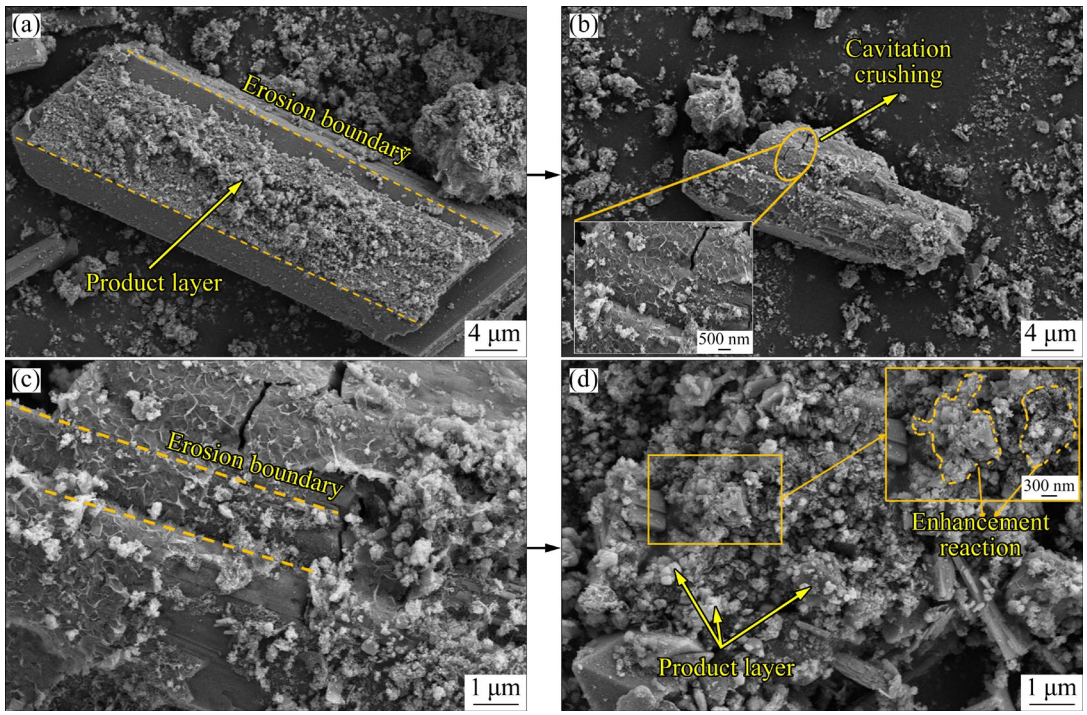

Fig. 8 SEM images of ZPRR after leaching under different conditions: (a) 100 °C, 0 W, 15 g/L H_2SO_4 and 240 min; (b, c) 100 °C, 360 W, 15 g/L H_2SO_4 and 240 min; (d) 150 °C, 360 W, 15 g/L H_2SO_4 and 240 min

diffusion into the internal reaction. When the 360 W ultrasonic field was applied, the dense layer covering the reacted ZPRR surface fractured, creating cracks, as shown in Fig. 8(b).

The cavitation effect of ultrasound generated numerous cavitation bubbles, releasing substantial energy upon rupture. The energy disturbed the thick surface layer on the surface of the ZPRR, enabling the enclosed elements to participate in the leaching reaction. In addition, the previously condensed and concentrated layer of the product changed, further reducing its thickness. This modification facilitated the entry of acid into the inner areas of the ZPRR, enabling further interactions with the enclosed phases and increasing leaching efficiency.

Figures 8(c, d) illustrate the impact of various reaction temperatures on the morphology of ZPRR. The experiment was conducted with an H_2SO_4 concentration of 15 g/L, a leaching time of 240 min, and applying a 360 W ultrasonic field to increase the leaching process.

As the temperature increases, the ZPRR surface reacts more intensely, resulting in a loose and porous structure. This occurs because higher leaching temperatures enhance the reactivity of the surface, leading to a faster and more thorough dissolution. Consequently, the enclosed phases within the ZPRR are exposed and can actively participate in the reaction.

A similar result was observed when Ga was leached using a solution of 150 g/L H_2SO_4 (Fig. S5 in SM). Additionally, the ZPRR surface exhibited a loose and porous structure after ultrasound treatment.

3.5.3 FT-IR spectra

FT-IR was used to observe the changes in the surface functional groups of ZPRR after acid leaching. The effect of ultrasound application on the surface functional groups of ZPRR after the reaction was examined under specific conditions. The temperature was 150 °C, the leaching time was 240 min, and H_2SO_4 concentrations were 15 and 150 g/L, respectively. Figure 9 illustrates the changes in the functional groups of ZPRR under these conditions.

Table 3 [35,48−52] presents the FT-IR data associated with the ZPRR. The antisymmetric absorption peak of O—H bonds is attributed to a small amount of moisture present in the material itself [48]. Fluctuations in this band are observed after applying ultrasound, indicating that the unique cavitation effect partially removes the product layer covering the reaction core. This is also due to an increase in reactive radicals, which creates a porous reaction surface and enhances the reactivity of the compounds in the solution [53].

Table 3 ZPRR-related FT-IR data

Functional group	Wavenumber/cm^{-1}	Ref.
O—H	3410.1	[48]
C═O	1625.2	[49]
SO_4^{2-}	1119.9	[50]
Al—O	815.3	[51]
SO_3^{2-}	673.9	[52]
S^{2-}	605.5	[53]
Si—O	798.0	[35]

The absorption peak of the C═O bond is caused by the existence of CO_2 in the surrounding atmosphere [49]. The absorption peak of SO_4^{2-} is caused by the presence of unreacted insoluble sulphate material in the ZPRR [50]. There are S^{2-} and SO_3^{2-} peaks which could indicate the presence of complex sulfur-containing compounds in the material [52]. This supports the effectiveness of leaching Ge at a concentration of 15 g/L H_2SO_4.

Figure 9(b) illustrates that a strong Si—O bond peak emerged in the presence of 150 g/L H_2SO_4 leaching. Conversely, the Si—O bond peak exhibited diminished intensity under 15 g/L H_2SO_4 leaching conditions. It is worthy that the structure of this silicate closely resembles that of silica gel [35]. The production of more silica gel at too high concentration of sulfuric acid (150 g/L) will inhibit the leaching of Ge.

4 Ultrasonic leaching mechanism

4.1 Crushing effect

Figure 10 illustrates the influence of leaching time on the structure of ZPRR. The experiment was conducted at a temperature of 130 °C, a H_2SO_4 concentration of 15 g/L, and an ultrasonic field of 360 W. Figure 10(a) demonstrates that after 60 min, ZPRR experienced the beneficial effect of cavitation induced by the ultrasonic field, resulting in noticeable surface cracks. However, the individual residue fragments remained relatively compact even after breaking. Figure 10(b) indicates that after

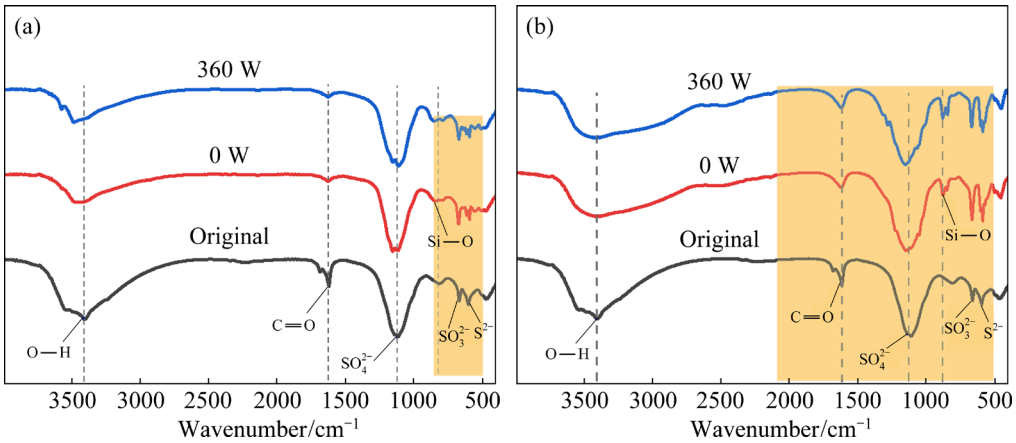

Fig. 9 FT-IR spectra of ZPRR after leaching at different H_2SO_4 concentrations: (a) 15 g/L H_2SO_4; (b) 150 g/L H_2SO_4

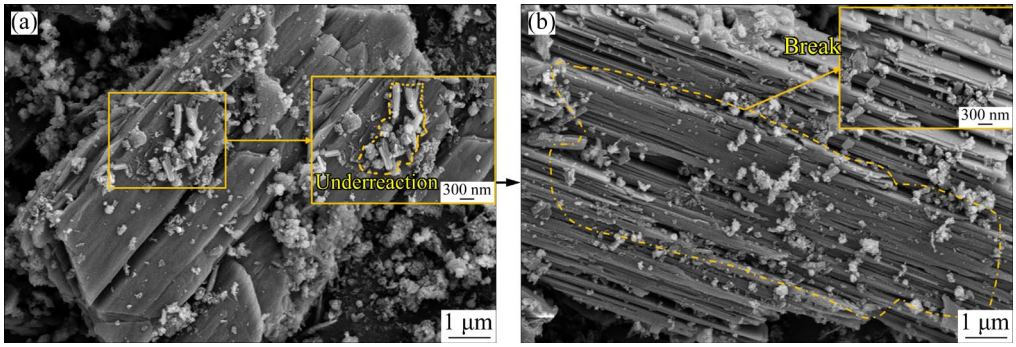

Fig. 10 SEM images of ZPRR under different leaching conditions: (a) 130 °C, 360 W, 15 g/L and 60 min; (b) 130 °C, 360 W, 15 g/L and 240 min

240 min of reaction, the dense surface of ZPRR became looser, and a more distinct laminar structure emerged. This indicates that the reaction of ZPRR became increasingly thorough as the leaching time was extended.

4.2 Dehydration effect

Additionally, it is worth noting that in a reaction environment where the L/S ratio is high (10 mL/g), the silicon in the leaching solution exists predominantly as H_4SiO_4, as indicated by the following reaction [8]:

$$Zn_2SiO_4 + 2H_2SO_4 \xrightarrow{\text{High L/S ratio}} 2Zn^{2+} + 2SO_4^{2-} + H_4SiO_4 \quad (3)$$

At elevated temperature and pressure, H_4SiO_4 undergoes dehydration processes [8]:

$$H_4SiO_4 \xrightarrow{\text{High temperature and pressure}} H_2SiO_3 + H_2O \quad (4)$$

$$H_2SiO_3 \xrightarrow{\text{High temperature and pressure}} SiO_2 + H_2O \quad (5)$$

Consequently, subjecting Ga and Ge to elevated temperature and pressure effectively prevents the formation of H_4SiO_4, reduces its preferential adsorption of Ge, and enhances its filtration capability to some extent [26].

The XPS was employed to analyze the impact of ultrasound on the elemental composition and electrochemical state of the ZPRR surface. Figure 11 displays the detailed spectrum of silicon in its original state within the ZPRR.

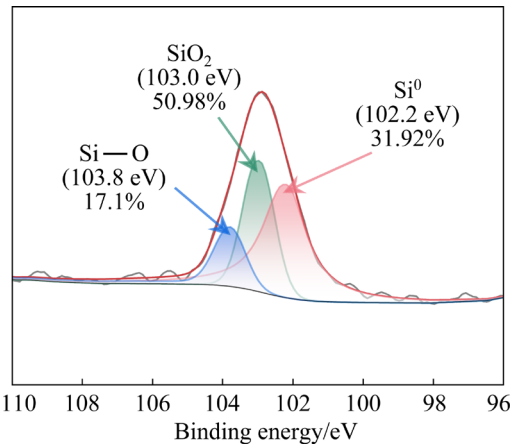

Fig. 11 XPS spectrum of Si 2p in original ZPRR

Table 4 [54−56] shows the binding energy of Si 2p from the original ZPRR. This suggests that Si in the original residue primarily exists as SiO_2, with a small amount of Si being influenced by moisture in the air and undergoing slight hydrolysis. These findings align with the results depicted in Fig. 2.

Table 4 XPS data of Si 2p from original ZPRR

Elemental state	Binding energy/eV	Ref.
Si—O	103.8	[54]
SiO_2	103.0	[55]
Si^0	102.2	[56]

Table 5 [57−59] shows that the binding energy of Si 2p in ZPRR under various acid-leaching conditions. Figure 12 shows that the application of 360 W ultrasound enhances the leaching process, resulting in a significant increase in the intensity of the SiO_3^{2-} peaks. This observation suggests that ultrasound facilitates the removal of water from silica gel under high temperature and pressure conditions. This finding aligns with the XRD results presented in Fig. 7.

Table 5 XPS data of Si 2p from leached ZPRR

Elemental state	Binding energy/eV	Ref.
Si—OH	103.8	[57]
Si—O—Si	103.2	[58]
SiO_3^{2-}	102.5	[59]

4.3 Promotion of Fe^{3+} reduction

Figure 13 displays the XPS spectrum of S 2p in the original ZPRR. Table 6 [60] shows the binding energy of S 2p from the original ZPRR. Figure 14 shows the results obtained after leaching under different conditions.

This increase signifies the intensity of the SO_4^{2-} peaks, as well as the formation of more $CaSO_4$ and $PbSO_4$. These findings align with Fig. 7. Based on Reaction (2), it can be inferred that additional H_2S was produced in the reactor. As shown in Fig. 1, the original ZPRR exhibited a high sulphide content. When subjected to ultrasonic-assisted leaching in an acidic environment, high levels of H_2S were generated. H_2S, functioning as a reductive gas, can efficiently convert Fe^{3+} in the solution to Fe^{2+}, thereby minimizing the formation of $Fe(OH)_3$ [50]. The existence of $Fe(OH)_3$ colloids

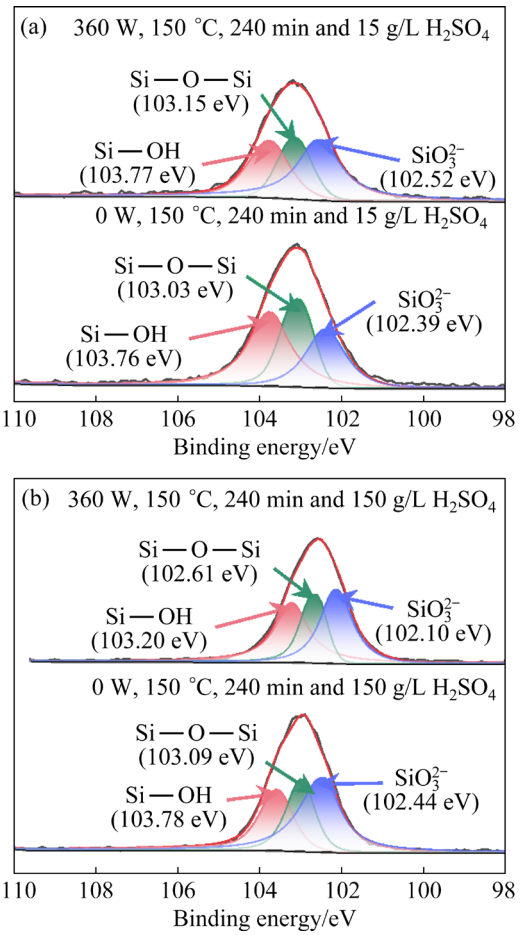

Fig. 12 XPS spectra of Si 2p of ZPRR leached under different conditions

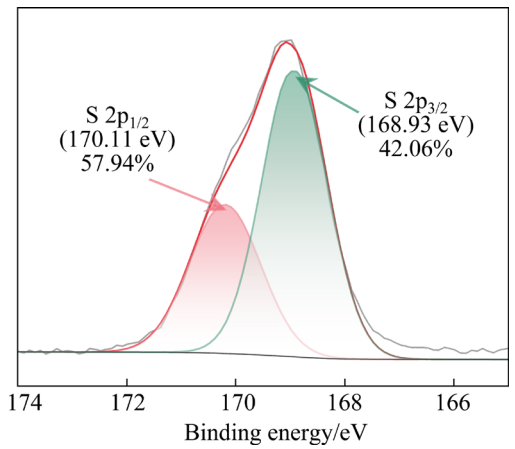

Fig. 13 XPS spectrum of S 2p in original ZPRR

results in the precipitation of iron [61], which exhibits selective adsorption behavior toward Ga and Ge, consequently reducing leaching efficiency. The reaction related to the reduction of Fe^{3+} is shown as follows [62]:

$$2Fe^{3+} + S^{2-} \rightarrow 2Fe^{2+} + 1/8S_8 \quad (6)$$

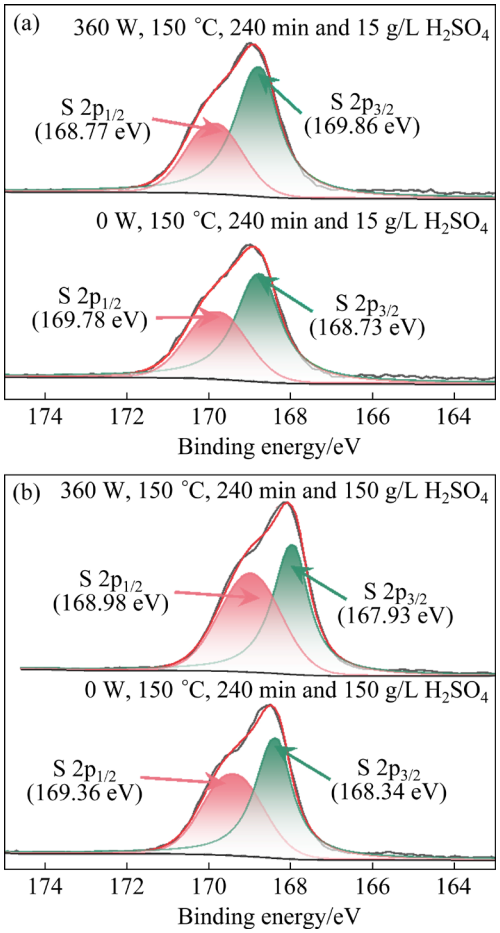

Fig. 14 XPS spectra of S 2p of ZPRR under different conditions

Table 6 XPS of S 2p data from original ZPRR

Elemental state	Binding energy/eV	Ref.
S $2p_{1/2}$	170.1	[60]
S $2p_{3/2}$	168.9	[60]

Subsequently, XPS was used to analyze the effect of ultrasonic application on the Fe 2p valence state under specific conditions: a reaction temperature of 150 °C, a leaching time of 240 min, and a H_2SO_4 concentration of 15 g/L. The results are presented in Fig. 15. In the absence of ultrasound, the Fe(III) exhibited asymmetrical Fe $2p_{3/2}$ and $2p_{1/2}$ peaks, accompanied by satellite peaks with significant binding energy.

Table 7 [63,64] clearly shows that the binding energy of Fe 2p in ZPRR under various acid leaching conditions.

It is evident that the Fe(II) eigen peak area accounts for 51.8% of the total, and when a 360 W ultrasonic field is applied, this proportion increases to 58.4%. This suggests that applying the ultrasonic field enhances the production of H_2S, which in turn promotes the reduction of Fe^{3+} to Fe^{2+}.

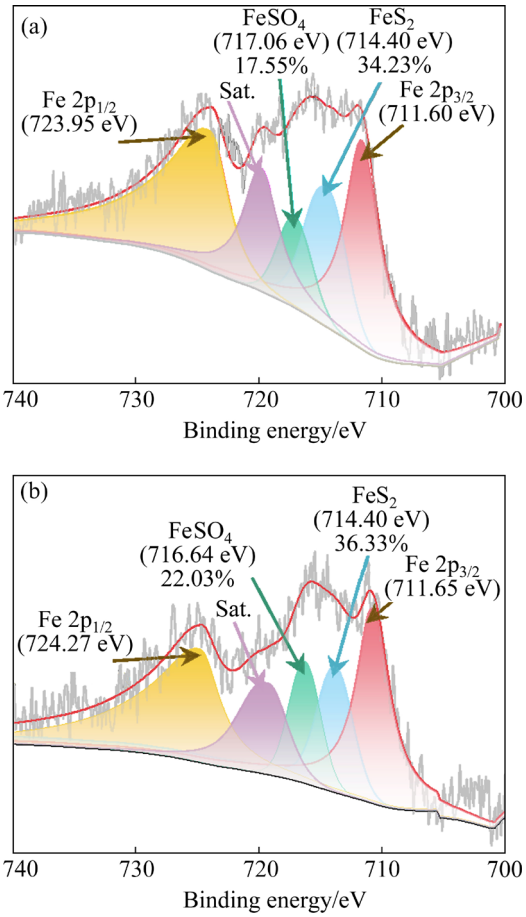

Fig. 15 XPS spectra of Fe 2p of ZPRR under different conditions: (a) 0 W, 15 g/L H_2SO_4 and 240 min; (b) 360 W, 15 g/L H_2SO_4 and 240 min

Table 7 XPS data of Fe 2p from leached ZPRR

Elemental state	Binding energy/eV	Ref.
Fe $2p_{3/2}$	711.6	[63]
Fe $2p_{1/2}$	723.9	[63]
$FeSO_4$	717.1	[64]
FeS_2	714.4	[64]

Although Fe^{2+} undergoes oxidation in an oxygen-rich environment, there is a competitive relationship between Fe^{2+} and oxygen. Additionally, the results demonstrate that the content of Fe^{2+} increases under ultrasonic treatment. Furthermore, Fe^{3+} can potentially be reduced by H_2S in the reaction environment. This evidence supports the conclusion that ultrasound makes the generation of more H_2S, thereby promoting the reduction process.

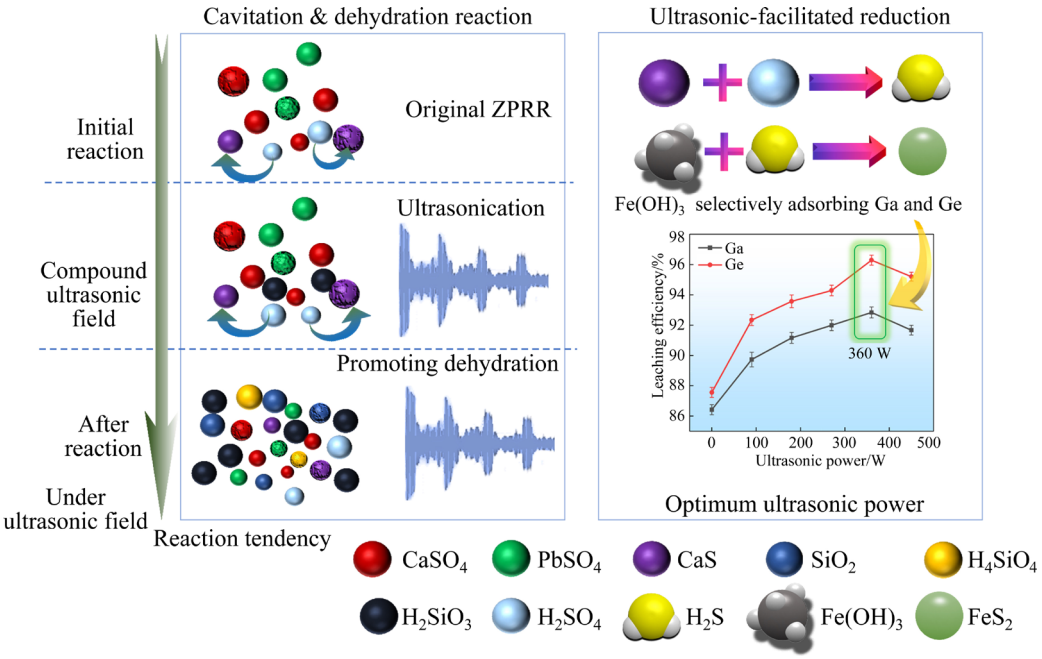

Fig. 16 Schematic diagram of ultrasonic leaching mechanism

The morphology and the distribution of elements in ZPRR were analyzed using SEM and EDS. The experiments were conducted at a reaction temperature of 150 °C, a leaching time of 240 min, a H_2SO_4 concentration of 15 g/L, and with or without the application of an ultrasonic field. The results are shown in Fig. S6 in SM. The Fe content in the leaching slag was observed to be 2.8 wt.% in the absence of an ultrasonic field. However, when applying a 360 W ultrasonic field, the Fe content decreased to 1.0 wt.%. This finding aligns with the XPS results, suggesting that the application of an ultrasonic field hindered the precipitation of iron. More Fe^{2+} ions were isolated from the solution.

Figure 16 presents a mechanism diagram of the ultrasonic field-enhanced leaching of Ga and Ge by the OPAL method, which offers a more comprehensive visualization of the facilitating role of the ultrasonic field in the reaction.

Ultrasound induces cavitation and mechanical effects that break down residue, disrupt the dense structure, and facilitate the formation of reactive radicals, resulting in a loose and porous surface. Furthermore, ultrasound accelerated the dehydration process of H_4SiO_4, reducing the adsorption of Ga and Ge due to silica gel polymerization. Additionally, it promotes the reduction of Fe^{3+}, preventing the formation of iron precipitates and ultimately increasing the leaching efficiencies of Ga and Ge. The optimal ultrasonic parameters were determined to be a frequency of 20 kHz, an ultrasonic power of 360 W, and a leaching temperature of 150 °C. These findings provide theoretical guidance for the process of extracting Ga and Ge using an ultrasonic field.

5 Conclusions

(1) In the ultrasound-enhanced selective leaching ZPRR process, there is a constraint relationship between ultrasonic power and leaching temperature. If the leaching temperature is too high, the cavitation effect of ultrasound will be weakened. The optimal leaching enhancement can be achieved when the reaction temperature is 150 °C, and the ultrasonic power is 360 W.

(2) The leaching process involved the extraction of Ge and Ga using different concentrations of H_2SO_4 (15 and 150 g/L) under specific conditions. These conditions included an ultrasonic power of 360 W, an ultrasonic frequency of 20 kHz, an agitation speed of 400 r/min, a leaching temperature of 150 °C, an oxygen pressure of 0.5 MPa, and a leaching time of 240 min. The achieved optimal leaching efficiencies for Ga and Ge were 95.7% and 94.5%, respectively.

(3) The application of SEM, XRD, EPMA, FT-IR and XPS verified that ultrasound enhances the leaching efficiencies of Ga and Ge by leveraging the

synergistic effects of cavitation and mechanical forces. In addition, ultrasonic efficiently disrupted the compact structure of the ZPRR, enabling the interior elements to actively engage in the reaction. Consequently, this increased the surface area of contact between the residue and the acid, facilitating the reaction. Ultrasound can decrease the thickness of the product layer, hence increasing the effectiveness of the reaction.

(4) The ultrasonic field significantly enhanced the chemical processes during the OPAL process. The use of an applied ultrasonic field improved the dehydration reaction of H_4SiO_4, significantly reducing the incidence of selective adsorption. Additionally, the ultrasonic field speeded up the breakdown of CaS and enhanced the generation of H_2S. Consequently, it assisted in further diminishing the presence of Fe^{3+}, inhibiting the formation of iron deposits, and reducing the specific attraction of Ga and Ge by $Fe(OH)_3$.

CRediT authorship contribution statement

Yuan-xin LIANG: Data curation, Formal analysis, Writing – Original draft; **Meng SUN:** Investigation; **Bo-yi LUO:** Data curation; **Biao DING:** Conceptualization, Writing – Review & editing; **Zhe SHEN:** Validation, Supervision; **Tian-xiang ZHENG:** Resources; **Qiang LI:** Resources; **Bang-fei ZHOU:** Resources; **Chun-mei LIU:** Validation; **Cai-gui WU:** Writing – Review & editing; **Wei-li REN:** Validation; **Yun-bo ZHONG:** Funding acquisition, Conceptualization, Supervision.

Declaration of competing interest

The authors declare that they have no known competing financial interest or personal relationships that could have appeared to influence the work reported in this paper.

Acknowledgments

This study was financially supported by the National Key Research and Development Program of China (No. 2022YFC2904900), the National Natural Science Foundation of China (Nos. 52204392, 52274385, 52204347), and the Young Elite Scientists Sponsorship Program by CAST, China (No. 2022QNRC001).

Supplementary Materials

Supplementary Materials in this paper can be found at: https://tnmsc.csu.edu.cn/download/20-p0956-2024-0897-Supplementary_Materials.pdf.

References

[1] TRUONG V K, HAYLES A, BRIGHT R, LUU T Q, DICKEY M D, KALANTAR-ZADEH K, VASILEV K. Gallium liquid metal: Nanotoolbox for antimicrobial applications [J]. ACS Nano, 2023, 17: 14406−14423.

[2] WANG Hong-zhang, CHEN Sen, ZHU Xi-yu, YUAN Bo, SUN Xu-yang, ZHANG Jie, YANG Xiao-hu, WEI Yen, LIU Jing. Phase transition science and engineering of gallium-based liquid metal [J]. Matter, 2022, 5: 2054−2085.

[3] ZHAO Zhi-bin, SONI S, LEE T, NIJHUIS C A, XIANG Dong. Smart eutectic gallium−indium: from properties to applications [J]. Advanced Materials, 2023, 35: e2203391.

[4] GENG Xi-lin, LIU Ying, ZHANG Wei, WANG Liang-shi, WEN Jian-kang, SUN Jian-zhi. Recent advances in the recovery of germanium during the zinc refining process [J]. Chemical Engineering Journal, 2022, 446: 137445.

[5] XU Zhi-peng, LIU Zuo-wei, GUO Xue-yi, LI Dong, ZOU Ming-Jin, TIAN Qing-hua. Gallium recovery by cyclone electrowinning from alkaline electrolyte with titanium cathode [J]. Transactions of Nonferrous Metals Society of China, 2024, 34(3): 1027−1036.

[6] LU Fang-hai, XIAO Tang-fu, LIN Jian, NING Zeng-ping, LONG Qiong, XIAO Li-hua, HUANG Fang, WANG Wan-kun, XIAO Qing-xiang, LAN Xiao-long, CHEN Hai-yan. Resources and extraction of gallium: A review [J]. Hydrometallurgy, 2017, 174: 105−115.

[7] ZHANG Wei, RAO Shuai, LI Li-qing, GONG Xiao-dan, WU Cai-gui, HU Dong-feng, CAO Hong-yang, LIU Zhi-qiang. Dissolution behavior and improvement approach for gallium extraction from zinc refinery residues [J]. Transactions of Nonferrous Metals Society of China, 2024, 34(3): 1016−1026.

[8] WU Xue-lan, WU Shun-ke, QIN Wwen-qing, MA Xi-hong, NIU Yin-jian, LAI Shao-shi, YANG Cong-ren, JIAO Fen, REN Liu-yi. Reductive leaching of gallium from zinc residue [J]. Hydrometallurgy, 2012, 113/114: 195−199.

[9] BAYAT S, AGHAZADEH S, NOAPARAST M, GHARABAGHI M, TAHERI B. Germanium separation and purification by leaching and precipitation [J]. Journal of Central South University, 2016, 23: 2214−2222.

[10] JIANG Tao, ZHANG Tao, LIU Zhi-hong. Review on resources and recycling of germanium, with special focus on characteristics, mechanism and challenges of solvent extraction [J]. Journal of Cleaner Production, 2021, 294: 126217.

[11] BRUNELLI K, DABALÀ M. Ultrasound effects on zinc recovery from EAF dust by sulfuric acid leaching [J]. International Journal of Minerals, Metallurgy, and Materials, 2015, 22: 353−362.

[12] FRENZEL M, KETRIS M P, SEIFERT T, GUTZMER J. On the current and future availability of gallium [J]. Resources Policy, 2016, 47: 38−50.

[13] LIU Fu-peng, LIU Zhi-hong, LI Yu-hu, LIU Zhi-yong, LI Qi-hou, ZENG Li. Extraction of gallium and germanium from zinc refinery residues by pressure acid leaching [J].

Hydrometallurgy, 2016, 164: 313−320.

[14] WU Ye-Hui-Zi, ZHOU Kang-gen, WEI Chen, LEI Qing-yuan, ZHANG Er-jun, CHENG Yu-yao, JIANG Yang, PENG Chang-hong, JIANG Jun, ZHANG Xue-kai. Chromatographic separation and recovery of Zn(II) and Cu(II) from high-chlorine raffinate of germanium chlorination distillation [J]. Transactions of Nonferrous Metals Society of China, 2022, 32(4): 1336−1350.

[15] GUI Qi-hao, HU Yu-ting, WANG Shi-xing, ZHANG Li-bo. Mechanism of synergistic pretreatment with ultrasound and ozone to improve gold and silver leaching percentage [J]. Applied Surface Science, 2022, 576: 151726.

[16] GUI Qi-hao, KHAN M I, WANG Shi-xing, ZHANG Li-bo. The ultrasound leaching kinetics of gold in the thiosulfate leaching process catalysed by cobalt ammonia [J]. Hydrometallurgy, 2020, 196: 105426.

[17] XIE Hui-min, XIAO Xi-yuan, GUO Zhao-hui, LI Shi-wei. One-stage ultrasonic-assisted calcium chloride leaching of lead from zinc leaching residue [J]. Chemical Engineering and Processing, 2022, 176: 108941.

[18] JOHN J J, HOUWER V D, MECHELEN D V, GERVEN T V. Effect of ultrasound on leaching of lead from landfilled metallurgical residues [J]. Ultrasonics Sonochemistry, 2020, 69: 105239.

[19] SHI Shen-chao, ZHONG Rui-zheng, LI Le-le, WAN Chi-dan, WU Can. Ultrasound-assisted synthesis of graphene@ MXene hybrid: A novel and promising material for electrochemical sensing [J]. Ultrasonics Sonochemistry, 2022, 90: 106208.

[20] WANG Zeng-jie, ZHOU Hong-peng, XUE Ji-lai, LIU Xuan, LIU Shi-zhe, LI Xiang, HE Ding-yong. Ultrasonic-assisted hydrothermal synthesis of cobalt oxide/nitrogen-doped graphene oxide hybrid as oxygen reduction reaction catalyst for Al−air battery [J]. Ultrasonics Sonochemistry, 2021, 72: 105457.

[21] RUČIGAJ A, CONNELL J G, DULAR M, GENORIO B. Influence of the ultrasound cavitation intensity on reduced graphene oxide functionalization [J]. Ultrasonics Sonochemistry, 2022, 90: 106212.

[22] NAVIK R, GAI Yan-zhe, WANG Wu-cong, ZHAO Ya-ping. Curcumin-assisted ultrasound exfoliation of graphite to graphene in ethanol [J]. Ultrasonics Sonochemistry, 2018, 48: 96−102.

[23] FAN Yang-yang, LIU Yan, NIU Li-ping, ZHANG Wei-guang, ZHANG Zi-mu. Reductive leaching of indium from zinc-leached residue using galena as reductant [J]. Minerals Engineering, 2021, 163: 106777.

[24] CHEN Yang-fan, TENG Wen-xin, FENG Xin, LI Jiang-ling, LIU Wei-zao, REN Shan, YANG Jian, LIU Qing-cai. Efficient extraction and separation of zinc and iron from electric arc furnace dust by roasting with $FeSO_4·7H_2O$ followed by water leaching [J]. Separation and Purification Technology, 2022, 281: 119936.

[25] ZHANG Ding-chuan, SUN Feng-long, ZHAO Zhong-wei, LIU Xu-heng, CHEN Xing-yu, LI Jiang-tao, HE Li-hua. Kinetics study on cobalt leaching from cobalt-bearing ternary sulfide in sulfuric acid solution under atmospheric pressure [J]. Transactions of Nonferrous Metals Society of China, 2024, 34(5): 1669−1680.

[26] LIANG Yuan-xin, LUO Bo-yi, ZHAO Lun, CHEN Liang-guo, DING Biao, SHEN Zhe, ZHENG Tian-xiang, GUO Yi-feng, LI Qiang, ZHOU Bang-fei, LIU Chun-mei, BRNIC J, REN Wei-li, ZHONG Yun-bo. Strong magnetic and ultrasonic fields enhanced the leaching of Ga and Ge from zinc powder replacement residue [J]. Separation and Purification Technology, 2024, 330: 125572 .

[27] LIU Xue, LIU Sen, YAN Ting-yu, WANG Zhong-rui, GAO Shu-tao, GAO Zhuo-you, NIE Xin-hao, LIU Ze-jiang. Isomorphous incorporation of tin ions into extra-large pore framework with high-stannum content as efficient Lewis acid catalyst [J]. Fuel, 2023, 340: 127505.

[28] KIM D, THISSEN P, VINER G, LEE D W, CHOI W, CHABAL Y J, LEE J B. Recovery of nonwetting characteristics by surface modification of gallium-based liquid metal droplets using hydrochloric acid vapor [J]. ACS Applied Materials & Interfaces, 2013, 5: 179−185.

[29] RAO Shuai, WANG Dong-xing, LIU Zhi-qiang, ZHANG Kui-fang, CAO Hong-yang, TAO Jin-zhang. Selective extraction of zinc, gallium, and germanium from zinc refinery residue using two stage acid and alkaline leaching [J]. Hydrometallurgy, 2019, 183: 38−44.

[30] DING Wei, BAO Shen-xu, ZHANG Yi-min, CHEN Bo, WAN Xue-li, XIAO Jun-hui. Innovative recovery of gallium and zinc from corundum flue dust by ultrasound-assisted H_2SO_4 leaching [J]. Mineral Processing and Extractive Metallurgy Review, 2024, 45(5): 495−508.

[31] RAFIEE P, GHASSA S, MOOSAKAZEMI F, KHOSRAVI R, SIAVOSHI H. Recovery of a critical metal from electronic wastes: Germanium extraction with organic acid [J]. Journal of Cleaner Production, 2021, 315: 128223.

[32] XU Ying-jie, XIA Hong-ying, ZHANG Qi, ZHANG Li-bo. An original strategy and evaluation of a reaction mechanism for recovering valuable metals from zinc oxide dust containing intractable germanide [J]. Journal of Hazardous Materials, 2024, 468: 133766.

[33] XU Ying-jie, XIA Hong-ying, ZHANG Qi, CAI Wu-chen, JIANG Gui-yu, ZHANG Li-bo. Efficient recovery of valuable metals from lead−zinc smelting by-products by ultrasonic strengthening [J]. Minerals Engineering, 2022, 190: 107915.

[34] JIA Li-juan, ZHONG Ying-ying, LI Kai, LI Bin, GAO Ji-yun, LIU Tian-cheng, WANG Fang, WU Wan-qin, FENG Jia-yu. Recovery of zinc resources from secondary zinc oxide via composite ammonia leaching: Analysis of Zn leaching behavior [J]. Chemical Engineering Journal, 2023, 472: 144930.

[35] LIU Fu-peng, LIU Zhi-hong, LI Yu-hu, WILSON B P, LIU Zhi-yong, ZENG Li, LUNDSTROM M. Recovery and separation of gallium(III) and germanium(IV) from zinc refinery residues. Part II: Solvent extraction [J]. Hydrometallurgy, 2017, 171: 149−156.

[36] LIU Fu-peng, LIU Zhi-hong, LI Yu-hu, WILSON B P, LUNDSTRöM M. Recovery and separation of gallium(III) and germanium(IV) from zinc refinery residues: Part I: Leaching and iron(III) removal [J]. Hydrometallurgy, 2017, 169: 564−570.

[37] XIN Chun-fu, XIA Hong-ying, JIANG Gui-yu, ZHANG Qi, ZHANG Li-bo, XU Ying-jie, CAI Wu-chen. Mechanism and kinetics study on ultrasonic combined with oxygen enhanced

leaching of zinc and germanium from germanium-containing slag dust [J]. Separation and Purification Technology, 2022, 302: 122167.

[38] HE Shan-ming, WANG Ji-kun, YAN Jiang-feng. Pressure leaching of high silica Pb-Zn oxide ore in sulfuric acid medium [J]. Hydrometallurgy, 2010, 104: 235−240.

[39] XU Ying-jie, XIA Hong-ying, ZHANG Qi, JIANG Gui-yu, ZHANG Li-bo, XIN Chun-fu, CAI Wu-chen. Ultrasonic enhanced hydrazine sulfate acid leaching of low-grade germanium dust [J]. Applied Energy, 2023, 332: 120485.

[40] CAI Zhi-hui, JIN Zhang-min, ZHU Lin-yi, LI Yue-bing, LEI Yue-bao, GAO Zeng-liang. Optimizing the calibration error of refraction angles in ultrasonic angle beam testing [J]. Sensors, 2020, 20: 1427.

[41] PHAN T H, KADIVAR E, NGUYEN V T, MOCTAR O E, PARK W G. Thermodynamic effects on single cavitation bubble dynamics under various ambient temperature conditions [J]. Physics of Fluids, 2022, 34: 023318.

[42] WANG Bao-wei, WANG Yu. A comprehensive review on persulfate activation treatment of wastewater [J]. Science of the Total Environment, 2022, 831: 154906.

[43] GĄGOL M, PRZYJAZNY A, BOCZKAJ G. Wastewater treatment by means of advanced oxidation processes based on cavitation—A review [J]. Chemical Engineering Journal, 2018, 338: 599−627.

[44] YU Yu-sen, CUI Li-xue, ZHANG Li-bo, WANG Yun-fan. Efficient mechanochemical leaching of zinc from zinc oxide ores [J]. Transactions of Nonferrous Metals Society of China, 2024, 34(6): 1976−1993.

[45] DONG Bin, GUO Yan-qing, YANG Jie, YANG Xiao-gang, WANG Lu-lu, HUANG De-chun. Turbulence induced shear controllable synthesis of nano $FePO_4$ irregularly-shaped particles in a counter impinging jet flow T-junction reactor assisted by ultrasound irradiation [J]. Ultrasonics Sonochemistry, 2023, 99: 106590.

[46] LIU Hong-liang, WANG Shi-xing, FU Li-kang, LE T, DAI Lin-qing, XIA Hong-ying, ZHANG Li-bo. High-efficiency recycling of copper-cadmium slag by ozonation with ultrasonic catalysis [J]. Separation and Purification Technology, 2023, 313: 123539.

[47] DEAN J A, Lange's handbook of chemistry [M]. Beijing: Science Press, 2003.

[48] TURKI A, OUDIANI A E, MSAHLI S, SAKLI F. Investigation of OH bond energy for chemically treated alfa fibers [J]. Carbohydrate Polymers, 2018, 186: 226−235.

[49] DONG Liang-min, JIAO Fen, LIU Wei, HUANG Ya-lin, WEI Xin, QIN Wen-qing. Separation of fluorine and aluminum from secondary aluminum dross by calcium-cured alkali roasting−water leaching [J]. Transactions of Nonferrous Metals Society of China, 2024, 34(6): 2007−2019.

[50] DEMIATE I M, DUPUY N, HUVENNE J P, CEREDA M P, WOSIACKI G. Relationship between baking behavior of modified cassava starches and starch chemical structure determined by FTIR spectroscopy [J]. Carbohydrate Polymers, 2000, 42: 149−158.

[51] SONG Lei-ting, DI Hao-kai, LIANG Ming, ZENG Yin-er, YANG Kun, ZHANG Li-bo. Study on ultrasonic depolymerization of Si−Ge precipitation in zinc oxide dust leaching process [J]. Arabian Journal of Chemistry, 2023, 16(8): 105016.

[52] KLOPROGGE J T, HICKEY L, FROST R L. FT-Raman and FT-IR spectroscopic study of synthetic Mg/Zn/Al-hydrotalcites [J]. Journal of Raman Spectroscopy, 2004, 35: 967−974.

[53] WANG Wen-bo, TIAN Guang-yan, ZHANG Zhi-fang, WANG Ai-qin. A simple hydrothermal approach to modify palygorskite for high-efficient adsorption of Methylene blue and Cu(II) ions [J]. Chemical Engineering Journal, 2015, 265: 228−238.

[54] ZATSEPIN D A, ZATSEPIN A F, BOUKHVALOV D W, GAVRILOV N V. Bi-doped silica glass: A combined XPS-DFT study of electronic structure and pleomorphic imperfections [J]. Journal of Alloys and Compounds, 2020, 829: 154459.

[55] SHUTTHANANDAN V, NANDASIRI M, ZHENG Jian-ming, ENGELHARD M H, XU Wu, THEVUTHASAN S, MURUGESAN V. Applications of XPS in the characterization of battery materials [J]. Journal of Electron Spectroscopy and Related Phenomena, 2019, 231: 2−10.

[56] PINTORI G, CATTARUZZA E. XPS/ESCA on glass surfaces: A useful tool for ancient and modern materials [J]. Optical Materials: X, 2022, 13: 100108.

[57] POCHE T, WIRTH W, JANG S. Chemical structure characteristics of flexible low-*k* SiCOH thin films etched by inductively coupled plasma-reactive ion etching process using FTIR and XPS spectra analysis [J]. Microelectronic Engineering, 2024, 292: 112221.

[58] BANERJEE J, BOJAN V, PANTANO C G, KIM S H. Effect of heat treatment on the surface chemical structure of glass: Oxygen speciation from in situ XPS analysis [J]. Journal of the American Ceramic Society, 2018, 101: 644−656.

[59] ZHANG Lu-lu, KURAMOTO N, AZUMA Y, KUROKAWA A, FUJII K. Thickness measurement of oxide and carbonaceous layers on a ^{28}Si sphere by XPS [J]. IEEE Transactions on Instrumentation and Measurement, 2017, 66: 1297−1303.

[60] KIM S S, BRITCHER L, KUMAR S, GRIESSER H J. XPS study of sulfur and phosphorus compounds with different oxidation states [J]. Sains Malays Siana, 2018, 47: 1913−1922.

[61] ZHANG Yu-juan, SUN Jun-min, LÜ Guo-zhi, ZHANG Ting-an, GONG Yan-bing. Kinetics of alumina extraction from coal gangue by hydrochloric acid leaching [J]. Transactions of Nonferrous Metals Society of China, 2023, 33(6): 1932−1942.

[62] RAABE T, RASSER H, NOTTELMANN S, GROß A, KRAUSE H, KURETI S. Mechanistic study on H_2S and subsequent O_2 adsorption on iron oxides and hydroxides [J]. Applied Surface Science, 2021, 565: 150504.

[63] MOREIRA G F, PEÇANHA E R, MONTE M B M, LEAL FILHO L S, STAVALE F. XPS study on the mechanism of starch-hematite surface chemical complexation [J]. Minerals Engineering, 2017, 110: 96−103.

[64] EGGLESTON C M, EHRHARDT J J, STUMM W. Surface structural controls on pyrite oxidation kinetics: An XPS-UPS, STM, and modeling study [J]. American Mineralogist, 1996, 81: 1036−1056.

超声强化氧压选择性浸出锌粉置换渣中 Ga 和 Ge 的机理

梁元鑫[1,2]，孙 猛[1,2]，罗博轶[1,2]，丁 彪[1,2]，沈 喆[1,2]，郑天祥[1,2]，
李 强[1,2]，周邦飞[1,2]，刘春梅[1,2]，吴才贵[3]，任维丽[1,2]，钟云波[1,2]

1. 上海大学 材料科学与工程学院，上海 201900；
2. 上海大学 省部共建高品质特殊钢全国重点实验室，上海 201900；
3. 深圳中金岭南有色金属有限公司 丹霞冶炼厂，韶关 512000

摘 要：通过超声辅助硫酸浸出，研究了锌粉置换渣中镓和锗的浸出机制。通过 XRD、SEM、XPS 和 FT-IR 表征发现，超声处理可促进 H_4SiO_4 胶体的脱水，从而降低其对镓和锗配合物的吸附能力。此外，超声还能增强 CaS 在 H_2SO_4 中的溶解，增加 H_2S 的生成，这有助于 Fe^{3+}的还原并抑制铁沉淀的形成。通过系统优化包括超声功率(0~450 W)、温度(100~120 ℃)和浸出时间(30~120 min)工艺参数，分别实现了镓和锗 95.7%和 94.5%的最佳浸出效率。

关键词：氧压酸浸；超声波处理；锌粉置换渣；镓；锗；浸出机理

(Edited by Wei-ping CHEN)